# A balanced clock: network plasticity in the central mammalian clock

Olde Engberink, A.H.O.

two

# BRIEF LIGHT EXPOSURE AT DAWN AND DUSK CAN ENCODE DAY LENGTH IN THE NEURONAL NETWORK OF THE MAMMALIAN CIRCADIAN PACEMAKER

Anneke H.O. Olde Engberink[1], Job Huisman[1], Stephan Michel[1*], Johanna H. Meijer[1*]

[1]Department of Cellular and Chemical Biology, Laboratory for Neurophysiology, Leiden University Medical Center, Einthovenweg 20, 2333 ZC, Leiden, the Netherlands.
*these authors share senior author

*Published in FASEB J., 2020, 34, 13685-13695*

## ABSTRACT

The central circadian pacemaker in mammals, the suprachiasmatic nucleus (SCN), is important for daily as well as seasonal rhythms. The SCN encodes seasonal changes in day length by adjusting phase distribution among oscillating neurons thereby shaping the output signal used for adaptation of physiology and behavior. It is well-established that brief light exposure at the beginning and end of the day, also referred to as "skeleton" light pulses, are sufficient to evoke the seasonal behavioral phenotype. However, the effect of skeleton light exposure on SCN network reorganization, remains unknown. Therefore, we exposed mice to brief morning and evening light pulses, that mark the time of dawn and dusk in a short winter- or a long summer day. Single-cell PER2::LUC recordings, electrophysiological recordings of SCN activity, and measurements of GABA response polarity revealed that skeleton light-regimes affected the SCN network to the same degree as full photoperiod. These results indicate the powerful, yet potentially harmful effects of even relatively short light exposures during the evening or night for nocturnal animals.

## 1. INTRODUCTION

The rotation of the earth around its axis, combined with the earth orbiting the sun causes both daily and seasonal changes in photoperiod, light intensity, temperature, and food availability. Many organisms have evolved an intrinsic clock that produces circadian rhythms that help anticipate these changes in the environment. In mammals, the central circadian clock resides in the suprachiasmatic nucleus (SCN) of the ventral hypothalamus and provides daily signals to downstream tissues (Ralph *et al.*, 1990; Hastings *et al.*, 2018). Individual SCN neurons generate autonomous circadian rhythms by a genetic feedback loop of clock genes and their protein products (Buhr & Takahashi, 2013). Intercellular interactions synchronize and stabilize the rhythms of cells within the network (Mohawk & Takahashi, 2011) and cause the SCN to produce a coherent signal of the ensemble. This signal is in turn synchronized to the ambient light-dark cycle through light information perceived by the retina and projects to the SCN via the retinohypothalamic tract.

The SCN adapts to photoperiodic changes in day length, and thereby acts not only as a daily pacemaker, but also as a seasonal pacemaker. Seasonal encoding is achieved by a compression of the distribution of single-cell patterns of electrical activity in short winter days, and decompression in long summer days (VanderLeest *et al.*, 2007; Brown & Piggins, 2009). The readjustment of phases within the SCN leads to an alteration in the ensemble waveform of SCN electrical activity (MUA) with a wider peak width in long days and a more narrow peak width in short days (Mrugala *et al.*, 2000). This SCN waveform is thus an internal representation of the length of the day, and leads to the proper seasonal adjustments in mammals.

The studies on seasonal encoding by the SCN have been an excellent example of the ability of integrated networks to perform tasks that exceed the ability of individual neurons within the network; while individual SCN neurons have the cell-autonomous ability to produce circadian rhythms, they require a functioning network to recognize and encode the length of the day. Proper recognition of the season by the SCN is, therefore, an emerging property of the network, rather than a single-cell property.

However, there has been a major shortcoming in the study on seasonal encoding. In laboratory conditions, nocturnal animals are routinely exposed to light for the full length of the day. In contrast, in nature these animals experience environmental light conditions that are far from that: they spend most of their days in dark burrows and see the light usually only during dusk and dawn. We have, therefore, undertaken an investigation in which we question whether the reception of the full photoperiod is necessary to achieve the cellular reorganization within the SCN. Early studies have shown that these "skeleton" photoperiods are sufficient for adaptation of behavioral activity in nocturnal rodents, with shorter duration of activity during short summer nights and longer activity duration during the winter nights (Pittendrigh & Daan, 1976; Rosenwasser *et al.*, 1983; Stephan, 1983). Whether skeleton photoperiods will also affect the phase-shifting responses to light pulses – clearly present in full photoperiod – and are sufficient to evoke the molecular and electrophysiological adaptations of the central circadian clock has not been studied.

In this study, we use skeleton photoperiods consisting of 30 minutes light exposure at the beginning and end of each day to mimic long days of 16 hours and short days of 8 hours.

Exposure to the skeleton photoperiod affected the circadian clock in a strikingly similar manner as a full photoperiod. At different levels ranging from behavioral to electrophysiological (spike impulse frequency) and molecular rhythms (single-cell PER2 expression), neurotransmitter function (GABA-action) and phase-shifting capacity, the characteristic responses of adaptation to photoperiod could be reproduced with exposure to light pulses marking the beginning and end of the day.

## 2. MATERIALS AND METHODS

### 2.1. Animals and behavioral activity recordings

All experiments were performed using either male wild-type mice of 2 – 5 months old (C57BL/6J, Envigo, Horst, the Netherlands) or male homozygous PERIOD2::LUCIFERASE (PER2::LUC) mice of 3 – 6 months old, the latter were backcrossed to C57bl/6 and bred at the Leiden University Medical Center animal facility (Buijink *et al.*, 2016). All animals were housed in climate-controlled cabinets with full-spectrum diffused lighting with an intensity between 50 and 100 lux (Osram truelight TL), and *ad libitum* access to food and water throughout the experiment. The mice were entrained to either a skeleton long or short photoperiod according to the following protocol (see Figure 1A): all animals were first placed in 12 hours light – 12 hours dark (LD 12:12) for at least 1 week, and then 1 week in a skeleton photoperiod 12:12 (LDLD 0.5:11:0.5:12). For the skeleton long photoperiod, mice were thereafter exposed for 7 - 10 days to a skeleton photoperiod 14:10 (LDLD 0.5:13:0.5:10), and subsequently for at least 4 weeks to a skeleton photoperiod 16:8 (LDLD 0.5:15:0.5:8). For the skeleton short photoperiod, mice were exposed for 7 days to a skeleton photoperiod 10:14 (LDLD 0.5:9:0.5:14), and finally at least 4 weeks to a skeleton photoperiod 8:16 (LDLD 0.5:7:0.5:16). Not all animals were able to entrain to a skeleton long photoperiod. It is a well-known phenomenon in the skeleton long photoperiod entrainment that the final reduction in "night" length to 8 hours can lead to unstable entrainment, and the mice then "phase-jump" to a more stable phase angle of entrainment, which then represents entrainment to a short skeleton photoperiod (Pittendrigh & Daan, 1976; Stephan, 1983). We excluded all data from this study from animals with unstable entrainment leading to a phase jump. During entrainment to the skeleton photoperiod, mice were housed individually and their cages were equipped with a running wheel and a passive infrared sensor (PIR) for recording locomotor and home-cage activity, respectively. Both the number of wheel revolutions and PIR data were recorded using ClockLab software (ClockLab; Actimetrics, Wilmette, IL). The PIR data were used as an extra control, in addition to the running wheel recordings, for the determination of entrainment. Activity onsets and offsets were determined during the last 14 days of each photoperiod by visual inspection of the actogram by three investigators independently. The average onset and offset as well as the duration of activity (alpha) were calculated in ClockLab. All animal experiments were performed in accordance with the regulations of the Dutch law on animal welfare, and the institutional ethics committee for animal procedures of the Leiden University Medical Center (Leiden, the Netherlands) approved the protocol (DEC 13198 and PE.18.113.004).

## 2.2. Behavioral experiments

For the phase-shifting experiments, mice were either entrained to skeleton long or short photoperiod as described above or for at least 28 days to full long (LD 16:8) or short (LD 8:16) photoperiod after which the animals were released into constant darkness (DD). On day 4 in DD, the animals received a 30 minutes white light pulse around circadian time 15 (CT15). CT12 was routinely defined as the time of the onset of activity. From each animal in the cabinet, the onset of activity was calculated at day 4 in DD, and the timing of the light pulse was determined such that most animals would receive the light pulse closest to CT15 (CT15 ± 1 h). The behavioral activity was recorded for another week after the light pulse. The phase shifts in the locomotor activity rhythm were calculated in ClockLab from the wheel running data by measuring the difference between fitted lines through the activity onsets in DD before and after the light pulse.

## 2.3. Bioluminescence imaging

PER2::LUC mice were entrained to skeleton long or short photoperiod as described above and were taken for experimentation after at least 28 days in the final photoperiod. Slice cultures of the SCN were prepared as previously described (Buijink *et al.*, 2016). In brief, mice were killed by decapitation within one to three hours before the projected night of the skeleton photoperiod. Decapitation and subsequent dissection of the brain took place in dim red light until the optic nerves were cut. The brain was dissected and placed in modified ice-cold artificial cerebrospinal fluid (ACSF), containing (in mM): NaCl 116.4, KCl 5.4, $NaH_2PO_4$ 1.0, $MgSO_4$ 0.8, $CaCl_2$ 1, $MgCl_2$ 4, $NaHCO_3$ 23.8, glucose 15.1, and 5 mg/L of gentamycin (Sigma Aldrich, Munich, Germany) and saturated with 95% $O_2$ – 5% $CO_2$. From each brain, two consecutive coronal slices (200 µm thick) of the hypothalamus containing the SCN were made with a vibrating microtome (VT 1000S, Leica Microsystems, Wetzlar, Germany). The slice containing the anterior SCN was optically identified, the subsequent slice was considered to contain the posterior SCN. From these slices, the SCN was isolated and two explant cultures were maintained on a Millicell membrane insert (PICMORG50, Merck – Millipore, Burlington, MA, USA) in a 35 mm dish containing 1.2 mL of Dulbecco's Modified Eagel's Medium supplemented with 10 mM HEPES buffer (Sigma-Aldrich, Munich, Germany), 2% B-27 (Gibco, Landsmeer, The Netherlands), 5 U/mL of penicillin, 5 µg/mL of streptomycin (0,1% penicillin-streptomycin; Sigma-Aldrich, Munich, Germany), and 0.2 mM D-luciferin sodium salt (Promega, Leiden, The Netherlands) and adjusted to pH 7.2 with NaOH. The dish containing the slices was sealed with a glass cover slip and transferred to a temperature-controlled (37 °C) and light-tight chamber (Life Imaging Services, Reinach, Switzerland), equipped with an upright microscope and a cooled CCD camera (ORCA –UU-BT-1024, Hamamatsu Photonics Europe, Herrsching am Ammersee, Germany). Bioluminescence images from the anterior and posterior SCN explants were acquired consecutively with an exposure time of 29 minutes resulting in image series with 1 hour time resolution.

### *Data analysis*

The image time series were analyzed using a custom-made, MATLAB-based (Mathworks, Natick, MA, USA) program, as described in (Buijink *et al.*, 2016). In brief, groups of pixels that showed

characteristics of single-cells were identified and these regions of interest (ROIs) will be referred to as single-cells. Single-cells were only used if the time series contained at least three cycles with periods between 18 and 30 hours, and with peaks above and troughs below the trend line. The processed intensity traces from the single-cell rhythms were evaluated on sustained PER2::LUC signal and circadian rhythm characteristics, like peak time and period. Phase distribution was defined as the standard deviation (SD) of the peak time from all cells per explant, of the first cycle in vitro. Single-cell period variability was defined as the cycle-to-cycle time difference between the half-maximum of the rising edge of the PER2::LUC expression rhythm. The variability in period is defined as the standard deviation (SD) of the cycle interval of individual cells, calculated for the first three cycles in vitro, and averaged per slice.

## 2.4. Ex vivo electrophysiology

Mice were entrained to skeleton long or short photoperiod as described above and were taken for experimentation after at least 28 days in the final photoperiod. The SCN slices were prepared during the light pulse that marks the end of the day. Coronal brain slices (~450 µm thick) were prepared using a tissue chopper, and the slice containing the SCN was transferred to a laminar flow chamber. The tissue was submerged into and continuously perfused (1.5 mL/min) with oxygenated regular ACSF ($CaCl_2$ increased to 2 mM and without $MgCl_2$, compared to modified ACSF, 35 ˚C, 95% $O_2$ and 5% $CO_2$). The slice was stabilized using an insulated tungsten fork and settled in the recording chamber for ~1 hour before the electrodes were placed in the center of the left and right SCN to obtain multiunit neuronal activity recordings from both nuclei. Action potentials were recorded using 75 µm 90% platinum/10% iridium electrodes. The signals were amplified (x10,000) by a high impedance amplifier (5112, Signal Recovery, Bracknell, UK) and bandpass filtered (0.3 Hz low-pass, 3 kHz high-pass). Action potentials were selected by a window discriminator and the ones that exceeded a predetermined threshold well above the noise (~5 µV) were counted in 10 seconds bins using a custom-made automated computer program.

### *Data analysis*

The electrophysiological data were analyzed using a custom-made program in MATLAB as described previously (VanderLeest *et al.*, 2007). The time of maximum activity was used as a marker of the phase of the SCN and was determined as the first peak in multiunit activity. Multiunit recordings of at least 24 hours in duration that expressed a clear peak in multiunit activity were moderately smoothed using a least-squares algorithm (Eilers, 2003). Subsequently, the SCN peak time, the peak width, and the relative peak amplitude (peak-to-trough ratio) of the first cycle ex vivo were determined.

## 2.5. $Ca^{2+}$ imaging

Mice were entrained to skeleton long or short photoperiod as described above and were taken for experimentation after at least 28 days in the final photoperiod. Decapitation and subsequent dissection of the brain were similar as described above for the bioluminescence experiments, with the exception that the slices made for $Ca^{2+}$ imaging were 250 µm thick. Slices were sequentially

maintained in regular, oxygenated ACSF. The slices were incubated in a water bath (37˚C) for 30 minutes and were then maintained at room temperature until the start of the recordings. Recordings were performed within a 4 hours interval centered around the middle of the projected day, referring to the previous light regime of the animal. Neurons in brain slices were bulk-loaded with the ratiometric, membrane permeable $Ca^{2+}$ indicator dye fura-2-acetoxymethyl ester (Fura-2-AM) as described previously (Michel *et al.*, 2013). Briefly, the slices were submerged into a mix of regular ACSF containing 7 µM Fura-2-AM for 10 minutes at 37˚C. The slices were then rinsed four times with fresh ACSF before being transferred to a recording chamber (RC-26G, Warner Instruments, Hamden, CT, USA) mounted on the fixed stage of an upright fluorescence microscope (Axioskop 2-FS Plus, Carl Zeiss Microimaging, Oberkochen, Germany) and constantly perfused with oxygenated ACSF (2.5 mL/min) at room temperature. The indicator dye was excited alternatively at wavelengths of 340 and 380 nm by means of a monochromator (Polychrome V, TILL Photonics; now FEI Munich GmbH, Munich, Germany). Emitted light (505 nm) was detected by a cooled CCD camera (Sensicam, TILL Photonics; now FEI Munich GmbH, Munich, Germany), and images were acquired at 2 seconds intervals. Using an eight-channel pressurized focal application system (ALA-VM8, ALA scientific instruments, NY, USA), GABA (200 µM, 15 s) was applied locally and neuronal responses were recorded as $Ca^{2+}$ transients. After two GABA pulses, which were separated by 1 minute baseline recording, ACSF containing elevated levels of $K^+$ (20 mM, 15 s) was applied to identify healthy, responding neurons. Cells with at least a 10% increase in $[Ca^{2+}]_i$ in response to high levels of $K^+$ were considered healthy cells. Both experiments and analysis were accomplished using imaging software (TILLvision, TILL Photonics; now FEI Munich GmbH, Munich, Germany).

### *Data analysis*

Single-wavelength images were background subtracted, and ratio images (340/380) were generated. Region of interest-defined cells and mean ratio values were determined, from which the intracellular $Ca^{2+}$ concentration was calculated. Neuronal $Ca^{2+}$ responses were further analyzed using IGOR Pro (WaveMetrics, Portland, OR, USA). The transient responses in $Ca^{2+}$ concentration within the first seconds after the stimulation were evaluated, with responses smaller than ± 10% of baseline values defined as non-responding cells. GABA-evoked responses showing $Ca^{2+}$ transients with a decrease in amplitude lower than 10% from baseline were considered inhibitory and responses with an increase higher than 10% from baseline were defined as excitatory. Cells that showed both excitatory and inhibitory responses after one GABA stimulation were defined as biphasic. Per animal, two to three SCN slices were analyzed and the $Ca^{2+}$ responses to GABA application were measured in 50 – 80 cells. For each animal, the distribution of the different types of responses and the E/I ratio were determined. To calculate the E/I ratio, the number of cells that responded excitatory was divided by the number of cells that responded inhibitory for each animal and averaged per group.

## 2.6. Statistics

Statistical analysis was performed using GraphPad Prism (San Diego, CA, USA) and RStudio (RStudio Team (2020). RStudio: Integrated Development Environment for R. RStudio, PBC, Boston,

MA, USA). The behavioral data on alpha and phase shifts and the electrophysiological data were analyzed with two-tailed student's *t*-tests. The effect of the skeleton long and short photoperiod on the distribution of GABAergic responses was tested using chi square tests. E/I ratio was tested with a two-tailed student's *t*-test. The bioluminescence data were analyzed using two-way ANOVAs with factors "photoperiod" (long or short) and "type" (full or skeleton) and in case of significance followed by a Sidak's correction for multiple comparisons. Last, the differences between the skeleton photoperiod and full photoperiod for the alpha, phase shifts, peak width, and PER2::LUC peak time SD were analyzed using two-way ANOVAs, type III, with factors "photoperiod" (long or short) and "type" (full or skeleton) and in case of significance followed by a Bonferroni correction for multiple comparisons. Differences with $P \leq 0.05$ were considered significant. All data are shown as mean ± SEM.

# 3. RESULTS

## 3.1. Exposure to a skeleton photoperiod changes behavioral activity patterns

We investigated whether C57BL/6 mice are able to adapt to different day lengths using only 30 minutes light pulses presented at the beginning and end of the day, so-called skeleton photoperiod. Wild-type mice were exposed to an entrainment paradigm in which they first were exposed to a 12:12 light-dark cycle, then to a 12:12 skeleton photoperiod, and next, the timing of the morning and evening light pulses shifted gradually until they were either representing a long (LD 16:8) or a short (LD 8:16) photoperiod. Exposure to skeleton photoperiods had a clear differential effect on the behavioral patterns of wheel-running activity in mice (Figure 1A and B). In both groups, mice continued to be active during the dark interval between the two light pulses in accordance with their previous night. Compressed and expanded durations of the active phase ($\alpha$) were observed under skeleton long and short photoperiods, respectively (Figure 1A and B, LP: $\alpha = 8.21 \pm 0.16$ h, n = 16, SP: $\alpha = 12.20 \pm 0.15$ h, n = 29, $P < 0.0001$). The circadian pattern of wheel-running activity in mice adapted to skeleton photoperiods corresponded with the previous reports using other rodents (Pittendrigh & Daan, 1976; Rosenwasser et al., 1983; Stephan, 1983) and thereby confirmed our experimental protocol. We also entrained wild-type mice to a full long and short photoperiod and the extent to which animals compressed or expanded their locomotor activity under skeleton photoperiods was quantitatively similar to the adaptation seen under full photoperiods (Figure S1A and (Refinetti, 2002; 2004; VanderLeest et al., 2007), full LP: $\alpha = 8.04 \pm 0.06$ h, n = 9, full SP: $\alpha = 12.24 \pm 0.31$ h, n = 10).

## 3.2. Phase-shifting capacity is different in mice adapted to a skeleton long vs short photoperiod

We next questioned how mice, once they were adapted to the skeleton photoperiod, would respond to phase-shifting light stimuli, since the maximum phase-shifting capacity depends strongly on the photoperiod to which animals are exposed (Refinetti, 2002; Evans *et al.*, 2004; vanderLeest *et al.*, 2009). To confirm the phase-shifting responses under full photoperiod (vanderLeest *et*

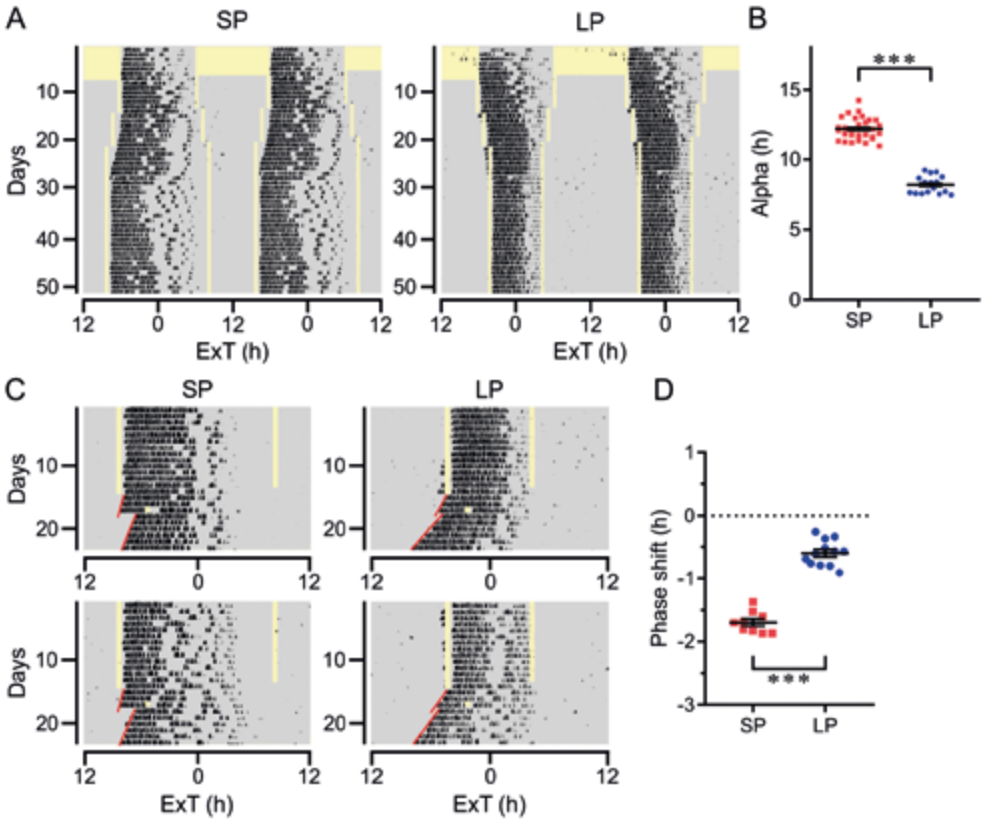


**Figure 1. Behavioral responses of mice entrained to the skeleton photoperiod.** A. Representative double–plotted actograms showing the locomotor wheel–running activity of a mouse during entrainment to skeleton short (left) and long (right) photoperiod. Grey areas represent darkness, yellow areas represent light. B. The duration of the activity phase (alpha) is higher in mice entrained to a skeleton short photoperiod compared to mice entrained to a skeleton long photoperiod. Data points shown are alphas calculated from all mice used for this study (both wild-type and PER2::LUC mice). C. Two representative single–plotted actograms showing the locomotor wheel-running activity in mice over the last 14 days of entrainment to a skeleton short (left) and long (right) photoperiod and the following DD period. On day 4 in DD, a light pulse was presented 3 hours after activity onset. Red lines are fitted through the activity onsets of the days in DD before and after the light pulse. Grey areas represent darkness, yellow areas represent light. D. The phase shift in response to a light pulse at ± CT15 is higher in mice entrained to a skeleton short photoperiod compared to mice entrained to a skeleton long photoperiod. *** $P < 0.0001$, t–tests. Error bars, mean ± SEM

*al.*, 2009), we first entrained mice to a full long and short photoperiod followed by three days in constant darkness and presented a light pulse at circadian time 15 (CT15) ± 1 hour, a time point known to produce the maximum delay (vanderLeest *et al.*, 2009). In mice entrained to long days by full photoperiod, light-induced phase delays were attenuated in comparison to mice entrained to short days (Figure S1B, LP: -0.13 ± 0.26 h, n = 7 vs. SP: -1.92 ± 0.10 h, n = 9, $P < 0.0001$). Next, we investigated whether these characteristic differences would hold under skeleton photoperiods. Therefore, mice received a light stimulus at CT15 ± 1 hour after entrainment to the skeleton photoperiod. Following

a skeleton short photoperiod, mice showed phase delays of ~1.7 hour in response to the light stimulus, whereas mice exhibited significantly smaller shifts of ~ 0.6 hour following adaptation to a skeleton long photoperiod (Figure 1C and D, LP: -0.60 ± 0.06 h, n = 12, SP: -1.69 ± 0.06 h, n = 9, $P < 0.0001$). The magnitude of the phase shifts is equal under a skeleton photoperiod compared to both long and short full photoperiod (Figure S1B, ns.). Both behavioral readouts of seasonal adaptation to full photoperiod, alpha and phase-shifting magnitude, are quite similar to our earlier studies ((VanderLeest et al., 2007) and (vanderLeest et al., 2009) respectively). The mechanisms underlying these behavioral changes are, therefore, only tested in skeleton photoperiods and compared with data from our previous studies generated under identical conditions. The phase-shifting capacity is intrinsic to the SCN and is explainable by the phase dispersal among SCN neurons, which is higher under a long photoperiod (vanderLeest et al., 2009). In full long photoperiod, phase dispersal of single-cell rhythms increases in the SCN and leads to a broader and more shallow waveform of the ensemble electrical activity (Mrugala et al., 2000; VanderLeest et al., 2007). Therefore, we next performed ex vivo experiments to test whether exposure to the skeleton photoperiod would suffice to encode day length in the SCN.

### 3.3. Waveform multiunit electrical activity (MUA) broadens under a skeleton long photoperiod

We measured the waveform and determined the peak width of the ensemble circadian MUA rhythm in SCN slices of mice entrained to a skeleton long or short photoperiod. A broader peak width corresponds with a wider phase distribution (Schaap *et al.*, 2003; VanderLeest *et al.*, 2007). Electrical recordings revealed high discharge rates during the projected day and low during the night, for both skeleton photoperiods. Peak time occurred about 1.5 hours before "midday", at circadian time (CT) 6.60 ± 0.51 h (n = 7) for a skeleton short photoperiod and CT 2.74 ± 0.87 (n = 7) for a skeleton long photoperiod. The waveform of SCN ensemble electrical activity showed a significantly broader peak when mice were entrained to a skeleton long photoperiod compared to a short photoperiod (Figure 2, LP: 12.48 ± 0.49 h, n = 7, SP: 10.03 ± 0.77 h, n = 7, $P < 0.05$). These results show a photoperiodic effect on the waveform, that is peak width, of electrical activity that is similar for the skeleton and full photoperiod (VanderLeest *et al.*, 2007).

### 3.4. Less GABAergic inhibition in mice entrained to a skeleton long photoperiod

We next investigated the effect of different skeleton photoperiods on GABAergic activity, by recording GABA-induced single-cell $Ca^{2+}$ transients in SCN slices from mice adapted to either skeleton long or short photoperiod (Figure 3A). $Ca^{2+}$ transients were categorized as inhibitory, excitatory, biphasic, or non-responder. The distribution of the different response types varied between recordings from animals entrained to skeleton long and short photoperiod. Adaptation to a skeleton long photoperiod decreased the GABA-induced inhibitory responses compared to short photoperiod (Figure 3B, 30% vs 37%, respectively; $P < 0.05$). Also, the percentage of GABAergic excitatory responses was higher than inhibitory responses in slices from a skeleton long photoperiod

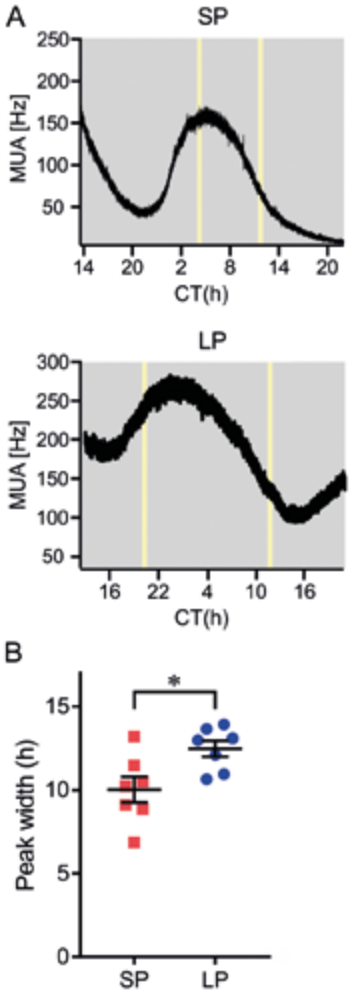


**Figure 2. Skeleton long photoperiod causes broadening of the ensemble electrical activity pattern of the SCN.** A. Example traces of ensemble electrical activity of the SCN in a slice from a mouse entrained to skeleton short (upper panel) and long (lower panel) photoperiod. The x–axis represents circadian time (CT 12 = onset of activity). Grey areas represent darkness, yellow areas represent light. B. The mean peak width of the ensemble electrical activity signal is higher in slices from mice entrained to a skeleton long photoperiod compared to slices from mice entrained to a skeleton short photoperiod. *$P$ < 0.05, t–test. Error bars, mean ± SEM

(Figure 3B, 39% vs. 30%, respectively; $P$ < 0.05). The mean excitatory/inhibitory (E/I) ratio was not significantly different between the skeleton photoperiods (Figure 3C, n.s.), but especially following a skeleton long photoperiod, the E/I balance was remarkably high (increased excitation), similar to full long photoperiod (Farajnia *et al.*, 2014). Thus, our results show that just the timing of two light pulses affects the polarity of responses to GABA.

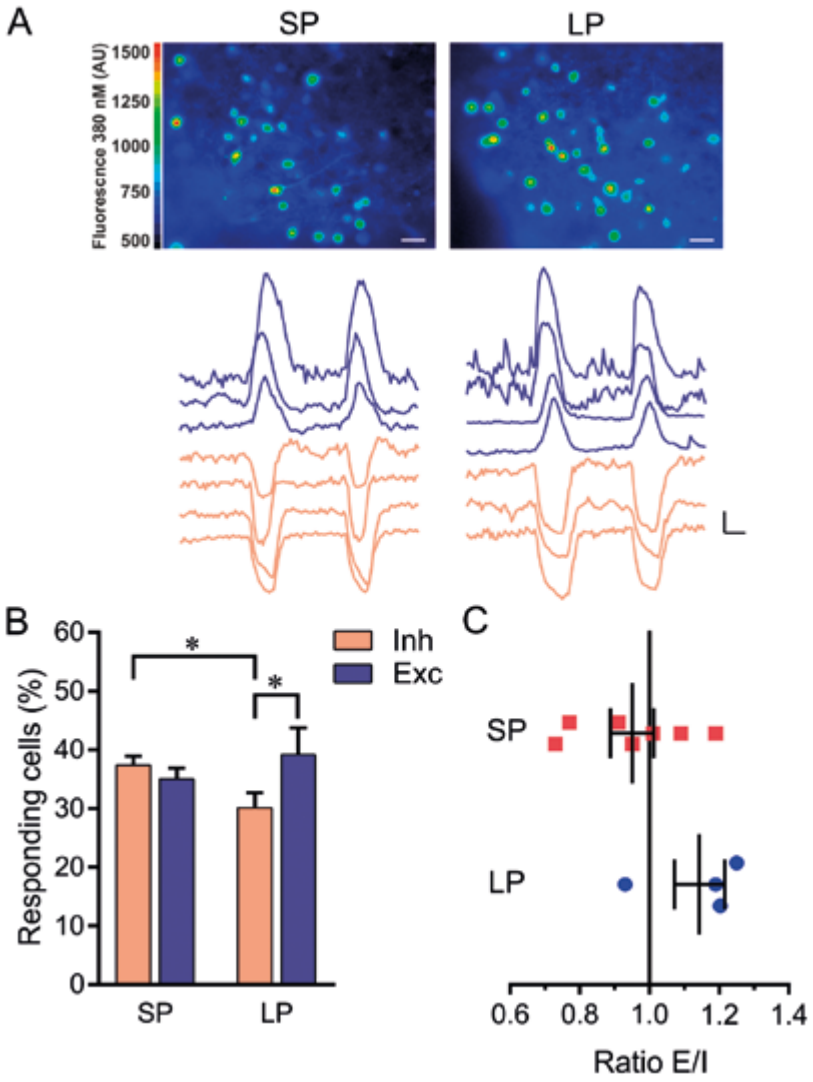


**Figure 3. Less GABAergic inhibition after entrainment to a skeleton long photoperiod.** A. Upper panels: examples of fura–2–AM loaded SCN neurons in slices from mice entrained to skeleton short (left) and long (right) photoperiod. Color scale indicates fluorescence at 380 nm excitation in arbitrary units (Scale bar, 20 μm). Lower panels: example traces Ca2+ transients in response to two GABA pulses recorded from one slice adapted to skeleton short (left) or long (right) photoperiod. Excitatory responses are shown in blue and inhibitory responses in orange (Scale bars, 20 nM, 20 s). B. The percentage of inhibitory responding cells is lower in slices from a skeleton long photoperiod compared to short photoperiod. The percentage excitatory responding cells in higher than inhibitory responding cells in slices from a skeleton long photoperiod. * $P < 0.05$, $\chi 2$ test. Error bars, mean ± SEM. C. The mean ratios of excitatory to inhibitory GABAergic signaling for skeleton short and long photoperiod do not differ. Each value indicates the ratio of all cells measured from one animal. n.s., t–test

### 3.5. Phase distribution of PER2::LUC rhythms is higher in mice entrained to a skeleton long photoperiod.

To test whether a skeleton photoperiod leads to changes in phase synchrony as under full photoperiod, we next performed ex vivo experiments to establish the phase distribution of SCN neurons. We performed PER2::LUC bioluminescence imaging experiments and measured single-cell PER2::LUC expression rhythms over multiple days in cultured anterior and posterior SCN explants from mice entrained to either skeleton long or short photoperiod (Figure 4A). We determined peak time and period of PER2::LUC rhythms from smoothed bioluminescence intensity traces of single SCN neurons. After adaptation to a skeleton long photoperiod, both the anterior and posterior part of the SCN showed a wider phase distribution of peak times compared to a skeleton short photoperiod.

Moreover, the anterior part of the SCN of mice entrained to a skeleton long photoperiod showed a higher peak time dispersion when compared to the posterior part (Figure 4B, LP: anterior: 3.23 ± 0.20 h, posterior: 1.76 ± 0.22 h, n = 6, SP: anterior: 1.08 ± 0.03 h, posterior: 1.12 ± 0.08 h, n = 7, $P < 0.05$). Furthermore, single-cell period variability – measured as the standard deviation (SD) of the cycle intervals of the first three cycles – was higher in both the anterior and posterior part of the SCN of mice entrained to a skeleton long photoperiod, compared to short photoperiod (Figure 4C, LP: anterior: 1.42 ± 0.08 h, posterior: 0.97 ± 0.10 h, n = 6, SP: anterior: 0.94 ± 0.03 h, posterior: 0.75 ± 0.02 h, n = 7, $P < 0.05$). This suggests that the increase in phase distribution was achieved by an increase in period variability of single neurons. Distribution of PER2::LUC rhythms were remarkably similar in the SCN of mice entrained to skeleton and full long photoperiod (Buijink et al., 2016).

## 4. DISCUSSION

Here, we show that exposure to a skeleton photoperiod affects the circadian clock in a similar manner as complete light exposure under a full photoperiod. At different levels ranging from behavioral to cellular and molecular, strikingly, nearly all characteristic responses to full photoperiod could be mimicked by just two 30 minutes pulses of light (Figure S1, (VanderLeest *et al.*, 2007; vanderLeest *et al.*, 2009; Farajnia *et al.*, 2014; Buijink *et al.*, 2016)). Exposure to a skeleton long photoperiod results in (a) complete adaptation of the behavioral activity pattern, (b) a reduction in the magnitude of phase delays in response to light pulses, (c) a broadening of the ensemble electrical activity pattern produced by the SCN ex vivo, (d) less GABAergic inhibitory responses in SCN neurons, and (e) desynchronization among oscillatory neurons, as revealed by single-cells *per2* clock gene expression. Moreover, the differences between a skeleton long photoperiod and skeleton short photoperiod were, for all parameters, concordant to the full photoperiods (see also Figure S1).

We entrained mice to full and skeleton long and short photoperiods and measured the extent to which animals compressed or expanded their duration of locomotor activity. The duration of wheel-running activity after adaptation to skeleton photoperiods is almost identical to our results obtained under full photoperiod (Figure S1A). Moreover, these results correspond qualitatively with those obtained in other rodent species and in Drosophilae (Pittendrigh & Minis, 1964; Pittendrigh

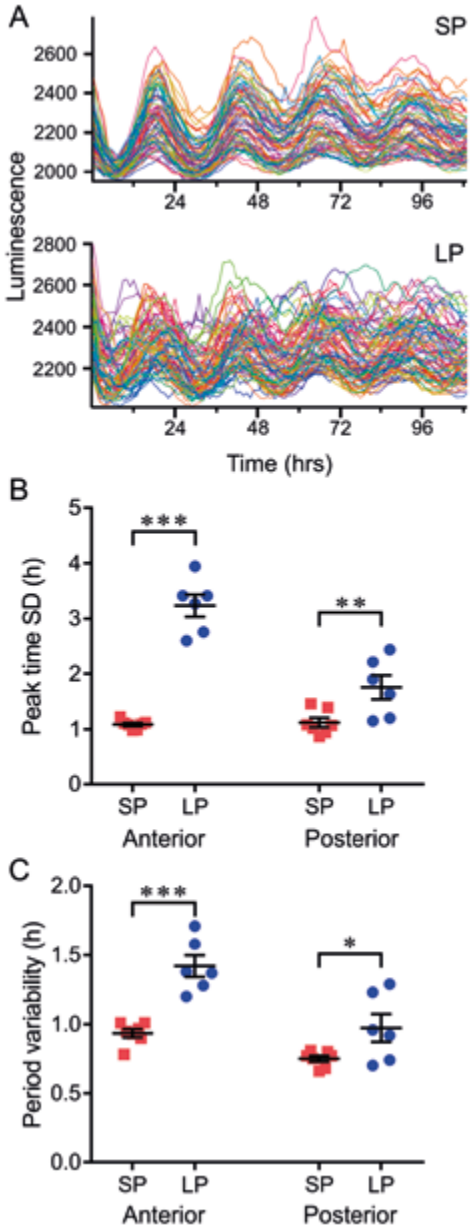


**Figure 4. Phase distribution of PER2::LUC rhythms is higher in mice entrained to a skeleton long photoperiod.** A. Examples of raw traces of bioluminescence intensity representing PER2::LUC expression from single cells in the anterior SCN of a mouse entrained to skeleton short (upper panel) and long (lower panel) photoperiod. The x–axis represents time in vitro after the start experiment. B. Phase distribution, defined by SD of peak times of the first cycle in vitro, is higher in both anterior and posterior SCN slices from mice entrained to a skeleton long photoperiod compared to short photoperiod. C. Period variability, defined as the SD of the cycle interval of individual cells over the first three cycles in vitro, is higher in both anterior and posterior SCN slices from mice entrained to a skeleton long photoperiod compared to short photoperiod. $^{*}P < 0.05$, $^{**}P < 0.01$, $^{***}P < 0.0001$, two–way ANOVAs with Sidak multiple comparisons tests. Error bars, mean ± SEM

& Daan, 1976; Rosenwasser *et al.*, 1983; Stephan, 1983). As under full photoperiod, we found that following adaptation to a skeleton photoperiod, the phase-shifting capacity is similarly reduced in short compared to long photoperiod (Figure S1B).

Behavioral adaptation to full photoperiods relies on a change in the degree of synchrony between the individual neurons (Quintero *et al.*, 2003; Schaap *et al.*, 2003; Yamaguchi *et al.*, 2003). Small neuronal subpopulations or single units in the SCN express only short durations of increased electrical activity and differ from one another in phase. The ensemble circadian waveform in electrical activity is composed of the sum of these neuronal activities (Mrugala *et al.*, 2000; Schaap *et al.*, 2003; Brown & Piggins, 2009). In full long photoperiod, the peak times in electrical activity in SCN neurons are more distributed over 24 hours, whereas the activity patterns from animals entrained to full short photoperiod are more synchronized (VanderLeest *et al.*, 2007; Brown & Piggins, 2009). Both in vivo and ex vivo, this results in a broad or narrow SCN multiunit activity pattern under long and short photoperiod, respectively (Mrugala *et al.*, 2000; Schaap *et al.*, 2003; VanderLeest *et al.*, 2007). We found that under skeleton photoperiods significant differences existed in the waveform of the SCN rhythm, with a compressed peak in a skeleton short photoperiod and a decompressed peak under a skeleton long photoperiod. As compared to results from previously published effects of a full long and short photoperiod on peak width, we show that the waveform of electrical activity is similarly affected by a skeleton and full photoperiod (skeleton LP: 12,48 ± 0,49 h, full LP: 11,76 ± 0,37 h, skeleton SP: 10,03 ± 0,77 h, full SP: 8,14 ± 0,33 h, factor "photoperiod" was significant: $P < 0.05$ for the skeleton and $P < 0.0001$ for full photoperiod, factor "type" [skeleton vs full] was ns both for LP and SP, two-way ANOVA followed by Bonferroni test (VanderLeest *et al.*, 2007)). Our data on waveform alterations suggest an underlying change in the phase distribution of SCN neurons.

We confirmed this by performing single-cell PER2::LUC bioluminescence recordings. A desynchronization of PER2 peak times was observed following a skeleton long photoperiod and more clustering in the phase following a skeleton short photoperiod. Responses of molecular rhythms to full photoperiodic exposure have also been shown for the clock genes *bmal1*, *per1*, and *per2* (Sumova *et al.*, 2004; Inagaki *et al.*, 2007; Naito *et al.*, 2008; Evans *et al.*, 2013; Myung *et al.*, 2015; Buijink *et al.*, 2016). It is well known that photoperiodic encoding at the molecular level relies on a different response of the anterior and the posterior SCN (Hazlerigg *et al.*, 2005; Inagaki *et al.*, 2007; Buijink *et al.*, 2016). We, therefore, tested whether a skeleton photoperiod leads to the same differential molecular response within the SCN. Indeed, we observed that the anterior SCN shows a significant higher phase dispersal under a skeleton long photoperiod compared to the posterior SCN, consistent with what we have shown earlier under full long photoperiod (skeleton LP: anterior: 3.23 ± 0.20 h, posterior: 1.76 ± 0.22 h, full LP: anterior: 3,42 ± 0,19 h, posterior: 1,81 ± 0,15 h, skeleton SP: anterior: 1.08 ± 0.03 h, posterior: 1.12 ± 0.08 h, full SP: anterior: 1,42 ± 0,04 h, posterior: 1,40 ± 0,13 h, factor "photoperiod" was significant: $P < 0.0001$ for skeleton and $P < 0.01$ for full photoperiod, factor "type" [skeleton vs full] was ns both for LP and SP, two-way ANOVA followed by Bonferroni test (Buijink *et al.*, 2016)). Specifically, we found a broad phase dispersal in the anterior SCN in response to light pulses at dawn and dusk similar to the responses measured in per1 and PER2 after full long photoperiods (Inagaki *et al.*, 2007; Buijink *et al.*, 2016).

The mechanisms that regulate neuronal phase distribution are still unknown, but the main neurotransmitter in the SCN – γ-Aminobutyric acid (GABA) – plays a role in phase adjustment and synchronization of the SCN neuronal network (Liu & Reppert, 2000; Albus *et al.*, 2005; Evans *et al.*, 2013; DeWoskin *et al.*, 2015; Myung *et al.*, 2015). Besides its classical inhibitory function, GABA has shown to also act as an excitatory neurotransmitter within the SCN (Wagner *et al.*, 1997; De Jeu & Pennartz, 2002; Albus *et al.*, 2005; Choi *et al.*, 2008; Irwin & Allen, 2009; Farajnia *et al.*, 2014). When exposed to full long photoperiod, the GABAergic E/I ratio shifts toward more excitation, suggesting a role for the E/I ratio in phase synchronization of individual SCN neurons (Farajnia *et al.*, 2014; Rohr *et al.*, 2019). Adaptation to a skeleton long photoperiod decreased the GABA-induced inhibitory responses compared to a skeleton short photoperiod and the percentage of GABAergic excitatory responses was higher than inhibitory responses in slices from a skeleton long photoperiod. Thus, exposure to the skeleton photoperiod is sufficient to affect the polarity of the GABAergic response and sufficient to adjust phase synchronization in the SCN neuronal network. However, E/I ratio under skeleton short photoperiod is higher when compared to a full short photoperiod (skeleton SP: 0.95 ± 0.06, full SP: 0.54), suggesting an additive effect of the full photoperiod light exposure on E/I balance. Given that the night-active rodents practically generate their own skeleton photoperiod by their behavior, it could be argued that the observed E/I balance and associated state of neuronal network is closer to their natural physiological conditions.

We conclude from our results that the continuous light-evoked neurotransmitter (ie, glutamate) release during the day is not required for coding photoperiod. Rather, we consider that the effects of light at the beginning and end of the animals' active period can be sufficient for photoperiodic adaptation by the SCN – from behavioral to cellular and molecular levels. This was unanticipated, because it is assumed that the characteristic of the SCN to respond tonically to light would be a prerequisite to adapt to the length of the day, thus requiring a full photoperiod (Yan & Silver, 2008). On the basis of the present results, our new hypothesis is that the phase delaying effect of light during dusk together with the phase advancing effect of light during dawn is sufficient to align the activity of SCN cells over the span of the day. This would agree with the concept of non-parametric entrainment, meaning that entrainment occurs on the basis of discrete phase shifts in response to pulses of light. The difference in the phase-shifting response that we observed between skeleton long and short photoperiod can accordingly be explained. Under a short photoperiod, when neurons are more synchronized in phase, a light pulse reaches all the single-cell oscillators at a similar phase leading the neurons to respond more coherent and resulting in a larger overall shift. In long day length, neurons are more desynchronized with a larger phase distribution, resulting in divergent phase-shifting responses and, as a consequence, a small overall shift (vanderLeest *et al.*, 2009).

The obvious question emerges whether the used skeleton light regime is merely an exotic paradigm used in laboratory research to unravel formal properties of clock cells, or whether there is also functional relevance. We argue that at least for nocturnal rodents the current protocol is possibly closer to the natural situation than full day light exposure. The behavior of many nocturnal animals sleeping underground during the day may already lead to a self-selected skeleton photoperiod with light exposures at the beginning and end of their active phase to mark the actual duration of the day.

And thus, exposure to full photoperiod, as is a general protocol in laboratory studies, may actually be less natural than exposure to a skeleton photoperiod. The results underscore the powerful effect of just brief pulses of light to achieve the full adjustment of the function of the SCN as a seasonal pacemaker.

Our findings are furthermore important given the use of electrical light at night, which is nowadays so abundantly present, especially in (sub)urban areas (Falchi *et al.*, 2016). This is particularly the case as the effects of long photoperiod can be completely mimicked by short pulses of light in the morning and evening, in about every single attribute of SCN organization and temporal behavior that we investigated. Even brief exposure to light, when animals get out of their burrows, can thus erroneously be interpreted as a sign for summer during winter time, leading to maladaptive physiological adaptation (such as the production of offspring at the wrong time of the year) (Russart & Nelson, 2018). There is mounting evidence that light at night disturbs the activity of nocturnal animal species including insects, showing the broad scale at which light pollution may be detrimental (Dominoni *et al.*, 2016; Knop *et al.*, 2017; Niepoth *et al.*, 2018; Sanders & Gaston, 2018). The fact that even brief light exposure can have physiological effects should be taken into consideration in light management programs aimed to preserve biodiversity.

## ACKNOWLEDGEMENTS

We thank Gabriella Lundkvist for providing PER2::LUC knock-in mice and Mayke Tersteeg for her technical assistance and help with animal caretaking. We also thank Ruben Schalk and Tom de Boer for their help with the statistics. This study was supported by funding from Velux Stiftung (project grant 1029 to SM) and by funding from ERC (adv grant 834513 to JHM)

## REFERENCES


1. Albus, H., Vansteensel, M.J., Michel, S., Block, G.D. & Meijer, J.H. (2005) A GABAergic mechanism is necessary for coupling dissociable ventral and dorsal regional oscillators within the circadian clock. *Curr. Biol.*, 15, 886-893.
2. Brown, T.M. & Piggins, H.D. (2009) Spatiotemporal heterogeneity in the electrical activity of suprachiasmatic nuclei neurons and their response to photoperiod. *J. Biol. Rhythms*, 24, 44-54.
3. Buhr, E.D. & Takahashi, J.S. (2013) Molecular Components of the Mammalian Circadian Clock. In Kramer, A., Merrow, M. (eds) *Circadian Clocks*. Springer Berlin Heidelberg, Berlin, Heidelberg, pp. 3-27.
4. Buijink, M.R., Almog, A., Wit, C.B., Roethler, O., Olde Engberink, A.H., Meijer, J.H., Garlaschelli, D., Rohling, J.H. & Michel, S. (2016) Evidence for Weakened Intercellular Coupling in the Mammalian Circadian Clock under Long Photoperiod. *PLoS One*, 11, e0168954.
5. Choi, H.J., Lee, C.J., Schroeder, A., Kim, Y.S., Jung, S.H., Kim, J.S., Kim, D.Y., Son, E.J., Han, H.C., Hong, S.K., Colwell, C.S. & Kim, Y.I. (2008) Excitatory actions of GABA in the suprachiasmatic nucleus. *J. Neurosci.*, 28, 5450-5459.
6. De Jeu, M. & Pennartz, C. (2002) Circadian modulation of GABA function in the rat suprachiasmatic nucleus: excitatory effects during the night phase. *J. Neurophysiol.*, 87, 834-844.
7. DeWoskin, D., Myung, J., Belle, M.D., Piggins, H.D., Takumi, T. & Forger, D.B. (2015) Distinct roles for GABA across multiple timescales in mammalian circadian timekeeping. *Proc. Natl. Acad. Sci. USA*, 112, E3911-3919.
8. Dominoni, D.M., Borniger, J.C. & Nelson, R.J. (2016) Light at night, clocks and health: from humans to wild organisms. *Biol. Lett.*, 12, 20160015.
9. Eilers, P.H. (2003) A perfect smoother. Anal. Chem., 75, 3631-3636.
10. Evans, J.A., Elliott, J.A. & Gorman, M.R. (2004) Photoperiod differentially modulates photic and nonphotic phase response curves of hamsters. *Am. J. Physiol. Regul. Integr. Comp. Physiol.*, 286, R539-546.
11. Evans, J.A., Leise, T.L., Castanon-Cervantes, O. & Davidson, A.J. (2013) Dynamic Interactions Mediated by Nonredundant Signaling Mechanisms Couple Circadian Clock Neurons. *Neuron*, 80, 973-983.
12. Falchi, F., Cinzano, P., Duriscoe, D., Kyba, C.C., Elvidge, C.D., Baugh, K., Portnov, B.A., Rybnikova, N.A. & Furgoni, R. (2016) The new world atlas of artificial night sky brightness. *Sci. Adv.*, 2, e1600377.
13. Farajnia, S., van Westering, T.L.E., Meijer, J.H. & Michel, S. (2014) Seasonal induction of GABAergic excitation in the central mammalian clock. *Proc. Natl. Acad. Sci. USA*, 111, 9627-9632.
14. Hastings, M.H., Maywood, E.S. & Brancaccio, M. (2018) Generation of circadian rhythms in the suprachiasmatic nucleus. *Nat. Rev. Neurosci.*, 19, 453-469.
15. Hazlerigg, D.G., Ebling, F.J.P. & Johnston, J.D. (2005) Photoperiod differentially regulates gene expression rhythms in the rostral and caudal SCN. *Curr. Biol.*, 15, R449-450.
16. Inagaki, N., Honma, S., Ono, D., Tanahashi, Y. & Honma, K.-i. (2007) Separate oscillating cell groups in mouse suprachiasmatic nucleus couple photoperiodically to the onset and end of daily activity. *Proc. Natl. Acad. Sci. USA*, 104, 7664-7669.
17. Irwin, R.P. & Allen, C.N. (2009) GABAergic signaling induces divergent neuronal Ca2+ responses in the suprachiasmatic nucleus network. *Eur. J. Neurosci.*, 30, 1462-1475.
18. Knop, E., Zoller, L., Ryser, R., Gerpe, C., Horler, M. & Fontaine, C. (2017) Artificial light at night as a new threat to pollination. *Nature*, 548, 206-209.
19. Liu, C. & Reppert, S.M. (2000) GABA synchronizes clock cells within the suprachiasmatic circadian clock. *Neuron*, 25, 123-128.
20. Michel, S., Marek, R., Vanderleest, H.T., Vansteensel, M.J., Schwartz, W.J., Colwell, C.S. & Meijer, J.H. (2013) Mechanism of bilateral communication in the suprachiasmatic nucleus. *Eur. J. Neurosci.*, 37, 964-971.
21. Mohawk, J.a. & Takahashi, J.S. (2011) Cell autonomy and synchrony of suprachiasmatic nucleus circadian oscillators. *Trends Neurosci.*, 34, 349-358.
22. Mrugala, M., Zlomanczuk, P., Jagota, A. & Schwartz, W.J. (2000) Rhythmic multiunit neural activity in slices of hamster suprachiasmatic nucleus reflect prior

photoperiod. *Am. J. Physiol. Regul. Integr. Comp. Physiol.*, 278, R987-994.

23. Myung, J., Hong, S., DeWoskin, D., De Schutter, E., Forger, D.B. & Takumi, T. (2015) GABA-mediated repulsive coupling between circadian clock neurons in the SCN encodes seasonal time. *Proc. Natl. Acad. Sci. USA*, 112, E3920-3929.
24. Naito, E., Watanabe, T., Tei, H., Yoshimura, T. & Ebihara, S. (2008) Reorganization of the suprachiasmatic nucleus coding for day length. *J. Biol. Rhythms*, 23, 140-149.
25. Niepoth, N., Ke, G., de Roode, J.C. & Groot, A.T. (2018) Comparing Behavior and Clock Gene Expression between Caterpillars, Butterflies, and Moths. *J. Biol. Rhythms*, 33, 52-64.
26. Pittendrigh, C.S. & Daan, S. (1976) A functional analysis of circadian pacemakers in nocturnal rodents. *J. Comp. Physiol.*, 106, 291-331.
27. Pittendrigh, C.S. & Minis, D.H. (1964) The Entrainment of Circadian Oscillations by Light and Their Role as Photoperiodic Clocks. *Am. Nat.*, 98, 261-294.
28. Quintero, J.E., Kuhlman, S.J. & McMahon, D.G. (2003) The biological clock nucleus: a multiphasic oscillator network regulated by light. *J. Neurosci.*, 23, 8070-8076.
29. Ralph, M.R., Foster, R.G., Davis, F.C. & Menaker, M. (1990) Transplanted suprachiasmatic nucleus determines circadian period. *Science*, 247, 975-978.
30. Refinetti, R. (2002) Compression and expansion of circadian rhythm in mice under long and short photoperiods. *Integr. Physiol. Behav. Sci.*, 37, 114-127.
31. Refinetti, R. (2004) Daily activity patterns of a nocturnal and a diurnal rodent in a seminatural environment. *Physiol. Behav.*, 82, 285-294.
32. Rohr, K.E., Pancholi, H., Haider, S., Karow, C., Modert, D., Raddatz, N.J. & Evans, J. (2019) Seasonal plasticity in GABA(A) signaling is necessary for restoring phase synchrony in the master circadian clock network. *eLife*, 8.
33. Rosenwasser, A.M., Boulos, Z. & Terman, M. (1983) Circadian feeding and drinking rhythms in the rat under complete and skeleton photoperiods. *Physiol. Behav.*, 30, 353-359.
34. Russart, K.L.G. & Nelson, R.J. (2018) Artificial light at night alters behavior in laboratory and wild animals. *J. Exp. Zool. A. Ecol. Integr. Physiol.*, 329, 401-408.
35. Sanders, D. & Gaston, K.J. (2018) How ecological communities respond to artificial light at night. Journal of experimental zoology. Part A, *Ecological and integrative physiology*, 329, 394-400.
36. Schaap, J., Albus, H., VanderLeest, H.T., Eilers, P.H., Detari, L. & Meijer, J.H. (2003) Heterogeneity of rhythmic suprachiasmatic nucleus neurons: Implications for circadian waveform and photoperiodic encoding. *Proc. Natl. Acad. Sci. USA*, 100, 15994-15999.
37. Stephan, F.K. (1983) Circadian rhythms in the rat: constant darkness, entrainment to T cycles and to skeleton photoperiods. *Physiol. Behav.*, 30, 451-462.
38. Sumova, A., Bendova, Z., Sladek, M., Kovacikova, Z. & Illnerova, H. (2004) Seasonal molecular timekeeping within the rat circadian clock. *Physiol. Res.*, 53 Suppl 1, S167-176.
39. VanderLeest, H.T., Houben, T., Michel, S., Deboer, T., Albus, H., Vansteensel, M.J., Block, G.D. & Meijer, J.H. (2007) Seasonal encoding by the circadian pacemaker of the SCN. *Curr. Biol.*, 17, 468-473.
40. vanderLeest, H.T., Rohling, J.H.T., Michel, S. & Meijer, J.H. (2009) Phase shifting capacity of the circadian pacemaker determined by the SCN neuronal network organization. *PLoS One*, 4, e0004976.
41. Wagner, S., Castel, M., Gainer, H. & Yarom, Y. (1997) GABA in the mammalian suprachiasmatic nucleus and its role in diurnal rhythmicity. *Nature*, 387, 598-603.
42. Yamaguchi, S., Isejima, H., Matsuo, T., Okura, R., Yagita, K., Kobayashi, M. & Okamura, H. (2003) Synchronization of cellular clocks in the suprachiasmatic nucleus. *Science*, 302, 1408-1412.
43. Yan, L. & Silver, R. (2008) Day-length encoding through tonic photic effects in the retinorecipient SCN region. *Eur. J. Neurosci.*, 28, 2108-2115.

## SUPPLEMENTARY MATERIALS



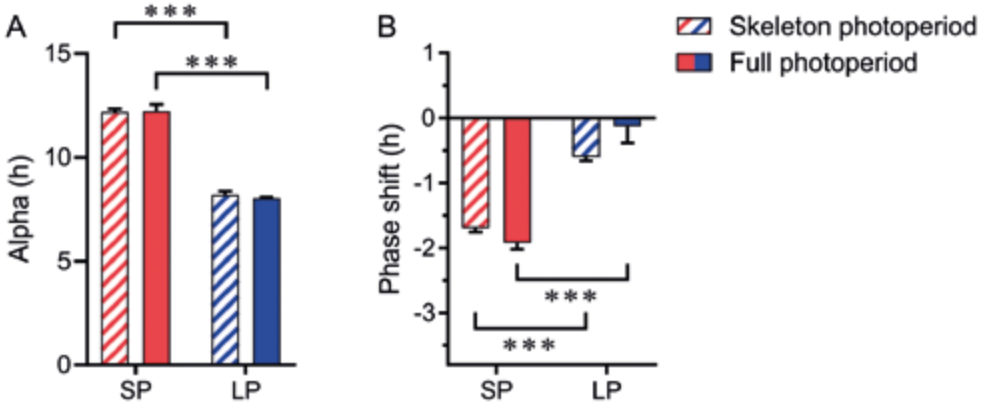


**Figure S1. Exposure to skeleton long photoperiod affects the circadian clock in a similar manner as complete light exposure under full long photoperiod.** A. The duration of activity phase (alpha) in mice entrained to skeleton and full, short and long photoperiod. Data for full photoperiod comes from animals that were used for phase shifting experiments. B. The mean phase shift in response to a light pulse at ± CT15 in mice entrained to skeleton and full, short and long photoperiod. Striped red bars = skeleton short photoperiod, striped blue bars = skeleton long photoperiod, red bars = full short photoperiod, blue bars = full long photoperiod. *** $P < 0.0001$, two-way ANOVAs with Bonferroni multiple comparison tests. Error bars, mean ± SEM.